High-order Eulerian methods for elastic-plastic flow in solids and coupling with fluid flows

By N. Ghaisas, A. Subramaniam AND S. K. Lele

1. Introduction

High-energy density materials undergoing large deformations occur in various problems of engineering interest which can benefit from a detailed understanding of the underlying physical processes, afforded by numerical simulations. Coupled solid-fluid interaction problems have been primarily simulated in either Lagrangian or Arbitrary Lagrangian-Eulerian frameworks. These methods encounter severe difficulties in problems involving large deformations, and a fully Eulerian method is well suited to such simulations (Plohr & Sharp 1989, 1992; López Ortega et al. 2014). The Eulerian equations tracking elastic and plastic flows in a single solid were developed by Plohr & Sharp (1989) and by Plohr & Sharp (1992). Although restricted to hyperelastic materials, a wide range of elastic and plastic behaviors can nevertheless be covered by these formulations (Miller & Colella 2001; Barton et al. 2013).

Barton et al. (2013) and López Ortega et al. (2014) extended the Eulerian formulation for elastic/plastic flow in a single solid to the case of multiple solids and fluids. The interface between materials was tracked via multiple level-set functions, and different equations were solved on different sides of the interface. A modified ghost fluid method (GFM) was used to enforce internal boundary conditions. This approach can be termed the 'sharp-interface' method, since each grid point was exclusively occupied by one material, and no 'mixing' of materials was allowed by this formulation. The GFM formulation is inherently non-conservative, and in problems involving interaction of shock waves and material interfaces, can possibly create spurious waves from the interfaces. An alternative approach, the so-called diffuse-interface method, was developed by Favrie & Gavrilyuk (2012) for two materials and extended to multiple materials by Ndanou et al. (2015). In this approach, the domain was composed of a mixture of materials characterized by the individual volume fractions which add up to one at each grid point. The same equations were solved over the whole domain, unlike in the sharp-interface method. This approach lends itself to use with high-order global numerical schemes such as compact finite-differences.

Solids undergoing large deformations display several features qualitatively similar to those observed in compressible fluids (Barton et al. 2013), and the governing equations of solids can be shown to be hyperbolic for certain equations of state and under certain constraints (Miller & Colella 2001). Previous attempts at solving these hyperbolic systems of equations relied either on Godunov-type methods (Trangenstein & Colella 1991; Miller & Colella 2001; Gavrilyuk et al. 2008; Barton et al. 2009), or on weighted essentially non-oscillatory (WENO) schemes (Hill et al. 2010; Barton et al. 2013; López Ortega et al. 2014) to handle strong discontinuities in the solution. Godunov-type methods require either approximate or exact Riemann solvers, which is complicated due to multitudes of possible equations of state, and by plasticity effects (Barton et al. 2013). Riemann solvers are also required to enforce internal boundary conditions in the sharp-interface multi-

material formulations (Barton et al. 2013; López Ortega et al. 2014) that use WENO for shock capturing. Godunov-type multi-material solvers are also difficult to extend to higher orders (Ndanou et al. 2015). WENO schemes, on the other hand, add excessive numerical dissipation, even in regions where the solution varies smoothly, and degrade the overall solution quality (Tritschler et al. 2014). This is especially problematic in situations involving turbulence, since the range of scales may be curtailed by such an excessively dissipative numerical scheme.

As an alternate shock-turbulence capturing scheme, the use of artificial fluid properties coupled with high-order compact finite-differences has been established as a successful method to achieve stable and accurate simulations while minimizing the numerical dissipation added at high wavenumbers (Cook & Cabot 2004; Kawai et al. 2010; Mani et al. 2009). Several formulations that provide strong damping of spurious oscillations near shocks while retaining high order of accuracy and low numerical dissipation in the rest of the domain have been developed and refined over the years, e.g., (Mani et al. 2009; Bhagatwala & Lele 2009; Olson & Lele 2011; Cook 2007). The motivation of this work is to develop a capability for Eulerian high-order simulations of elastic-plastic flow in solids, coupled to flow in fluids. In view of the challenges associated with Godunov-type and WENO methods referred to above, the use of artificial properties with compact finite-difference schemes is proposed here. The multi-material formulation of Favrie & Gavrilyuk (2012) and Ndanou et al. (2015) is suitable for this purpose, since interface tracking and other geometrical features are handled in a straightforward manner. This approach satisfies our need for high-order acccuracy and the ability to handle multiple materials undergoing large deformations.

The single and multi-material formulations are described first, followed by the numerical solution methodology, in Section 2. A few test problems that highlight some of the issues with the constitutive modeling of solids and the numerical solution of the governing equations are discussed in Section 3. A few preliminary results of multi-material elastic-plastic flow of solids are also described. The document ends with a brief summary and perspectives for ongoing work.

2. Formulation

2.1. *Single material formulation*

The fundamental equations of continuum mechanics include those governing conservation of mass, momentum and total energy,

$$\frac{\partial \rho}{\partial t} + \frac{\partial \rho u_k}{\partial x_k} = 0, \tag{2.1}$$

$$\frac{\partial \rho u_i}{\partial t} + \frac{\partial \left(\rho u_k u_i - \sigma_{ik}\right)}{\partial x_k} = 0, \tag{2.2}$$

$$\frac{\partial \rho \left(\varepsilon + \frac{1}{2}u_i^2\right)}{\partial t} + \frac{\partial \left(\rho \left(\varepsilon + \frac{1}{2}u_i^2\right) u_k - \sigma_{ik}u_i\right)}{\partial x_k} = 0. \tag{2.3}$$

These equations are similar to the Euler equations of fluid motion, with t and x_i being the time and space coordinates, respectively, and ρ, u_i, ε and σ_{ij} the density, velocity, internal energy and the Cauchy stress, respectively. Deformations of solids are described by the inverse deformation gradient tensor, defined as $g_{ij} = \partial X_i/\partial x_j$, where x_i and X_i are the positions of a continuum particle in the Eulerian and Lagrangian frames of reference, respectively. A multiplicative decomposition of the inverse deformation gradient tensor is

assumed, $g_{ij} = g^p_{il} g^e_{lj}$, such that g^e_{ij} tracks the elastic component of the total deformation while g^p_{ij} tracks the plastic component of the deformation. The equations governing g^e_{ij} can be written as (López Ortega et al. 2014; Ndanou et al. 2015)

$$\frac{\partial g^e_{ij}}{\partial t} + \frac{\partial u_k g^e_{ik}}{\partial x_j} = u_k \left(\frac{\partial g^e_{ik}}{\partial x_j} - \frac{\partial g^e_{ij}}{\partial x_k} \right) + \mathrm{L}^p_{ik} g^e_{kj}. \tag{2.4}$$

The $\partial/\partial t$ terms in eq. (2.4) are partial derivatives with respect to time with the Eulerian coordinates x_i (and not the Lagrangian coordinates X_i) held fixed. L^p_{ik} accounts for plasticity effects and is modeled as $\mathrm{L}^p_{ik} = \frac{1}{\tau_{rel}} g^e_{im} \sigma'_{mn} \left(g^e\right)^{-1}_{nk}$, with τ_{rel} a relaxation time parameter. $\sigma'_{mn} = \sigma_{mn} - \sigma_{kk}/3$ is the deviatoric part of the Cauchy stress. The first term on the right-hand side is added to ensure that the compatibility conditions (reflective of the fact that each row of g_{ij} is a gradient), $\bigtriangledown \times \mathbf{g} = \mathbf{0}$, be satisfied.

2.2. *Equation of state*

An equation of state (EOS) is required to close the above system of equations. In this study, we consider hyperelastic materials, or materials for which the constitutive behavior is defined by a strain energy density function. In particular, we consider an EOS which involves two components of internal energy: the hydrodynamic component and the elastic energy component, as (Ndanou et al. 2015)

$$\varepsilon = \varepsilon_h(\rho, \eta) + \varepsilon_e(\hat{\mathbf{g}}, \eta). \tag{2.5}$$

The hydrodynamic component depends only on the density and the entropy (η), while the elastic component depends on the deformations, with the tensor $\hat{\mathbf{g}} = |\mathbf{G}|^{-1/3}\mathbf{G}$ a scaled form of the inverse of the left Cauchy-Green tensor, $\mathbf{G} = \mathbf{g}^{eT}\mathbf{g}^e$. $|\mathbf{G}|$ denotes the determinant of the matrix $\mathbf{G}$. The expression for the hydrodynamic part of internal energy is analogous to a stiffened gas

$$\varepsilon_h = \frac{p + \gamma p_\infty}{(\gamma - 1)\rho} = \frac{A f(\eta) \rho^\gamma + (\gamma - 1) p_\infty}{(\gamma - 1)\rho}, \tag{2.6}$$

where the pressure $p = A f(\eta) \rho^\gamma - p_\infty$, A and $f(\eta)$ are a constant and an undefined function of entropy, respectively, p_∞ (units of pressure) and γ (non-dimensional) are material constants which determine the response of the material to extensional stress. Restricting the EOS to only the hydrodynamic component (i.e., neglecting the elastic component) reduces the material to a stiffened gas.

A dependence of internal energy on deformation via a non-zero ε_e accounts for resistance to shear loading of the material and distinguishes the system from a purely fluid system. The dependence of the elastic component of internal energy on the deformations can be expressed in many different ways. In this study, the expression is taken to be

$$\varepsilon_e = \frac{\mu}{4\rho_0} tr\left(\left(\hat{\mathbf{g}} - \mathbf{I} \right)^2 \right), \tag{2.7}$$

where μ is the shear modulus, ρ_0 is the density of the material in its undeformed state and tr denotes the trace of a tensor.

One advantage of this form of the separable EOS described above is that the Cauchy stress can be written out analytically as

$$\sigma = -p\mathbf{I} - \mu \frac{\rho}{\rho_0} \left(|\mathbf{G}|^{-2/3} dev\left(\mathbf{G}^2\right) - |\mathbf{G}|^{-1/3} dev\left(\mathbf{G}\right) \right), \tag{2.8}$$

where $dev(\mathbf{G})$ denotes the deviatoric part of the tensor $\mathbf{G}$.

2.3. *Multi-material formulation*

The extension of the above formulation to a problem involving L materials involves the continuum equations for conservation of mass, momentum and energy, Eqs. (2.1)-(2.3), with the mixture density, energy and Cauchy stress defined as

$$\rho = \sum_{l=1}^{L} \alpha^l \rho^l \quad \rho\varepsilon = \sum_{l=1}^{L} \alpha^l \rho^l \varepsilon^l \quad \sigma_{ij} = \sum_{l=1}^{L} \alpha^l \sigma_{ij}^l. \tag{2.9}$$

Each material $l = 1, 2, ..L$ in the mixture is defined by its individual volume fraction, α^l, density, ρ^l, internal energy, ε^l, Cauchy stress, σ_{ij}^l, pressure, p^l, and elastic part of the inverse deformation gradient, $g_{ij}^{e,l}$. The mixture is assumed to be described by one unique velocity field. The equations governing the volume fractions, mass fractions, hydrodynamic energies and deformations for each species are

$$\frac{\partial \alpha^l}{\partial t} + u_k \frac{\partial \alpha^l}{\partial x_k} = \frac{\left(p_I - p^l\right)}{\tau^l}, \tag{2.10}$$

$$\frac{\partial \alpha^l \rho^l}{\partial t} + \frac{\partial \alpha^l \rho^l u_k}{\partial x_k} = 0, \tag{2.11}$$

$$\frac{\partial \alpha^l \rho^l \varepsilon_h^l}{\partial t} + \frac{\partial \alpha^l \rho^l \varepsilon_h^l u_k}{\partial x_k} + \alpha^l p^l \frac{\partial u_k}{\partial x_k} = -\frac{p_I \left(p_I - p^l\right)}{\tau^l}, \tag{2.12}$$

$$\frac{\partial g_{ij}^{e,l}}{\partial t} + \frac{\partial u_k g_{ik}^{e,l}}{\partial x_j} = u_k \left(\frac{\partial g_{ik}^{e,l}}{\partial x_j} - \frac{\partial g_{ij}^{e,l}}{\partial x_k} \right) + \mathrm{L}_{ik}^{p,l} g_{kj}^{e,l}, \tag{2.13}$$

where p_I is an interfacial pressure and τ^l is a pressure relaxation time scale for material l. The introduction of the source terms involving p_I and τ^l in equations for the volume fractions and species hydrodynamic energies makes this a 'non-equilibrium' model, as oppposed to an 'equilibrium' model (Ndanou et al. 2015). The non-equilibrium model is motivated by the so-called six-equation model of Saurel et al. (2009), and is preferred over the equilibrium model as it leads to efficient means to ensure equality of pressures across materials at each point in the domain. Each material is also described by its own EOS of the form (2.5), with its own γ^l, p_∞^l and μ^l. In short, a total of $12L + 5$ equations need to be solved for a multi-material problem involving L species.

2.4. *Numerical solution*

The equations described above were discretized using tenth-order compact finite-difference schemes (Lele 1992) for all spatial derivatives. Derivatives at the boundaries were computed using either third-order one-sided compact differences constructed to maintain global conservation (Lele 1992) or using ghost points populated with appropriate symmetry or anti-symmetry conditions. The use of ghost points allows for the use of the same tenth-order stencil at the boundaries as at the interior points. Time advancement was done using a five-stage fourth-order Runge-Kutta method. Each stage of the Runge-Kutta algorithm entailed three steps: the hyperbolic update, wherein all source terms were neglected; the plastic relaxation, which accounted for the plastic source terms in the $g_{ij}^{e,l}$ equations; and the pressure relaxation, which adjusted the volume fractions, species densities and hydrodynamic internal energies so as to equilibrate species pressures (Favrie & Gavrilyuk 2012; Ndanou et al. 2015). An eighth-order compact filter was applied to all conserved variables after each step in each stage of the Runge-Kutta method (Cook 2007). Finally, in order to enable the use of compact finite-differences on fields involving

shocks, artificial shear and bulk viscosities, thermal conductivity and species diffusivities were employed in the momentum, species and mixture energies, and species mass fraction equations, respectively. The localized artificial diffusivity formulation described in Kawai et al. (2010) was used for the first three artificial properties, and the species mass fraction diffusivities were computed according to Cook (2007). The plastic relaxation and pressure relaxation steps were carried out as described in detail in Ndanou et al. (2015).

3. Preliminary results

The above algorithm is to be eventually implemented in three dimensions and applied to practical problems. In this document, preliminary results from a few test problems are described. These test problems highlight some issues with the theoretical formulation as well as pointing out and addressing some challenges with applying the above-mentioned numerical algorithm to the equations governing multi-material elastic-plastic flow of solids and fluids.

3.1. *Linear P and S waves*

For infinitesimal disturbances about an equilibrium medium at rest, the non-linear effects (including plasticity) are expected to be small. Linear elastic wave problems were considered first. Considering a 1D strain (P) wave with only diagonal stresses and deformation in the g_{11} component alone, the matrices

$$\mathbf{g} = \begin{bmatrix} g_{11} & 0 & 0 \\ 0 & 1 & 0 \\ 0 & 0 & 1 \end{bmatrix}, \quad \mathbf{G} = \begin{bmatrix} g_{11}^2 & 0 & 0 \\ 0 & 1 & 0 \\ 0 & 0 & 1 \end{bmatrix}, \quad \mathbf{G^2} = \begin{bmatrix} g_{11}^4 & 0 & 0 \\ 0 & 1 & 0 \\ 0 & 0 & 1 \end{bmatrix}.$$

Thus, $|\mathbf{G}| = g_{11}^2$ and the pressure was $p = Af(\eta)\rho_0^\gamma g_{11}^\gamma - p_\infty$. Ensuring $p = 0$ for $g_{11} = 1$ led to $Af(\eta)\rho_0^\gamma = p_\infty$ and hence, $p = p_\infty(g_{11}^\gamma - 1)$. The resulting Cauchy stress components were

$$\sigma_{11} = -p_\infty(g_{11}^\gamma - 1) - \frac{2}{3}\mu\left(g_{11}^{11/3} - g_{11}^{-1/3} - g_{11}^{7/3} + g_{11}^{1/3}\right)$$
$$\sigma_{22} = \sigma_{33} = -p_\infty(g_{11}^\gamma - 1) + \frac{1}{3}\mu\left(g_{11}^{11/3} - g_{11}^{-1/3} - g_{11}^{7/3} + g_{11}^{1/3}\right).$$

Writing the above equation for the Cauchy stress in terms of the longitudinal strain, using $g_{11} = (1 + \epsilon_{11})^{-1}$, and invoking the assumption $|\epsilon_{11}| \ll 1$ for infinitesimal disturbances, the stress components simplified to

$$\sigma_{11} = \left(\gamma p_\infty + \frac{4}{3}\mu\right)\epsilon_{11} \quad \sigma_{22} = \sigma_{33} = \left(\gamma p_\infty - \frac{2}{3}\mu\right)\epsilon_{11}.$$

Comparison to the general Hooke's law, $\sigma_{ij} = \lambda_L \epsilon_{kk}\delta_{ij} + 2\mu_L\epsilon_{ij}$, yielded the equivalent Lamé coefficients

$$\mu_L = \mu, \quad \lambda_L = \gamma p_\infty - 2\mu/3, \tag{3.1}$$

and the equivalent Young's modulus (E_L) and Poisson's ratio (ν_L) as

$$E_L = \mu_L \frac{3\lambda_L + 2\mu_L}{\lambda_L + \mu_L}, \quad \nu_L = \frac{\lambda_L}{2(\lambda_L + \mu_L)}. \tag{3.2}$$

A similar analysis of linear 1D shear (S) waves also led to the same expressions for the Lamé coefficients, Young's modulus and Poisson's ratio.

Given the equivalent Lamé coefficients, the one-dimensional linear strain and shear

TABLE 1. Separable EOS parameters used in literature and equivalent Young's moduli, E, and Poisson's ratios, ν. Negative ν was observed for three of the five parameter combinations.

Reference	Material Name	Separable EOS Parameters			Equivalent Parameters		Yield Stress σ_Y
		μ	γ	p_∞	E_L	ν_L	
Kluth & Despres (2008)	Steel	77 GPa	2.84	0.6 GPa	14 GPa	-0.907	2.49 GPa
Gavrilyuk et al. (2008)	'S1'	10 GPa	4.4	0.6 GPa	13.3 GPa	-0.337	∞
-	'S2'	5 GPa	2.4	0.6 GPa	6.95 GPa	-0.305	∞
Gavrilyuk et al. (2008)	Aluminium	26 GPa	3.4	21.5 GPa	69.7 GPa	0.341	0.2976 GPa
Favrie & Gavrilyuk (2010)	Copper	92 GPa	4.22	34.2 GPa	227 GPa	0.237	2.49 GPa

waves propagate with speeds $c_L = \sqrt{(\lambda_L + 2\mu_L)/\rho_0}$ and $c_T = \sqrt{\mu_L/\rho_0}$, respectively. Linear strain waves defined by the exact solution

$$\sigma_{11} = -\sigma_0 e^{-100(-(x-c_L t-0.5))^2}, \qquad \sigma_{22} = \sigma_{33} = \frac{\lambda_L}{\lambda_L + 2\mu_L}\sigma_{11},$$
$$\epsilon_{11} = \frac{1}{(\lambda_L + 2\mu_L)}\sigma_{11}, \qquad u = -\frac{c_L}{(\lambda_L + 2\mu_L)}\sigma_{11},$$

and linear shear waves defined by the exact solution

$$\sigma_{12} = \sigma_{21} = \sigma_0 e^{-100(-(x-c_T t-0.5))^2}, \quad \epsilon_{12} = \epsilon_{21} = \sigma_{12}/\mu_L, \quad v = \frac{c_T}{\mu_L}\sigma_{12}$$

were simulated on a periodic domain $x \in [0, 1]$. All other components of stress and strain tensors were trivial. The EOS parameters were $\gamma = 4.0, p_\infty = 6 \times 10^8$ Pa and $\mu = 10^{10}$ Pa. Figure 1 compares the velocity and stress components obtained at a certain time instant from the solution to the full one-dimensional equations and the solution of the linear one-dimensional wave propagation equation. As expected, the non-linear errors were small when $\sigma_0 = 10^6$ Pa$\sim 0.01 p_\infty$ (Figure 1), but were significant when $\sigma_0 \sim p_\infty$ (not shown). The error norms displayed the expected tenth-order of accuracy (not shown here) for these simple problems, thus serving as a verification for the numerical code.

A few typical EOS parameter values used in several previous studies (Gavrilyuk et al. 2008; Favrie & Gavrilyuk 2010) employing the separable EOS, along with the ostensibly represented material, are tabulated in Table 1. The equivalent Young's modulus and Poisson's ratio are also listed in Table 1. It was observed that while the equivalent E_L and ν_L values were meaningful in some cases, some parameter values yielded negative Poisson's ratios, which are not consistent with the behavior of metals subjected to infinitesimal stresses and strains (typically $\nu_L \sim 0.3 - 0.4$ for metals). The separable EOS parameters, namely γ, p_∞ and μ, tuned so as to obtain the correct behavior under finite deformations, thus were found to lead to spurious behavior under infinitesimal deformations.

The above discussions underscore the importance of choosing parameter values appropriately, such that the EOS is meaningful in infinitesimal as well as finite wave limits.

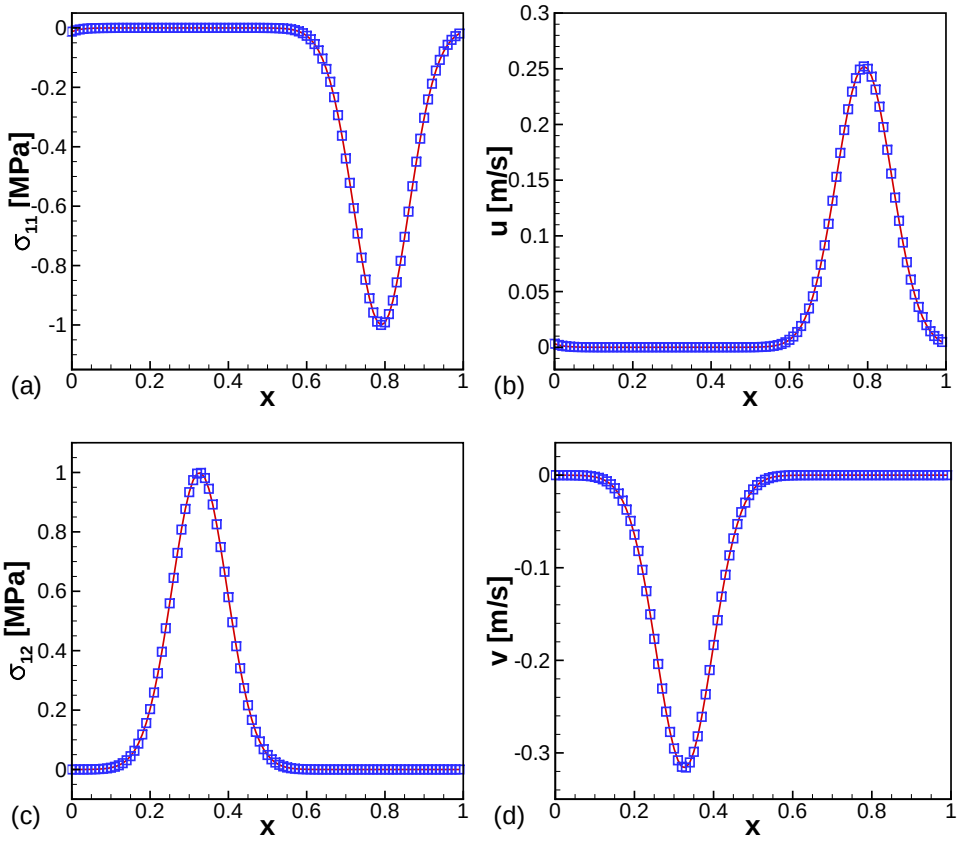

FIGURE 1. One-dimensional linear waves with strength $\sigma_0 = 10^6$ Pa, solved using the full non–linear equations (solid red lines) compared to the analytical solution of the linearized problem (blue squares). (a) Normal stress and (b) normal velocity for strain (P) waves, and (c) shear stress and (d) tangential velocity for shear (S) waves at $t = 0.5775$ ms. Material properties were $\gamma = 4.0, p_\infty = 6 \times 10^8$ Pa and $\mu = 10^{10}$ Pa. Numerical parameters were $NX = 101$ and $CFL = 0.5$.

One way to achieve this for the present separable EOS is to compute values for μ, γ and p_∞ from Eqs. (3.1) and an additional constraint, say $c_s = \sqrt{\gamma(p + p_\infty)/\rho}$, where c_s is an experimentally measured speed of sound in the medium at a given pressure p and density ρ. Similar constraints can be used to limit the parameter values ocurring in other equations of state (e.g., Godunov-Romenski, Dorovskii et al. (1983) or Neo-Hookean, Miller & Colella (2001)) to ensure meaningful behavior in the limit of small deformations.

3.2. *Stationary normal shock*

Any central differencing-based derivative calculation method gives rise to spurious Gibbs oscillations when applied to fields containing sudden jumps, or shocks. Artificial fluid properties were used previously (e.g., Cook (2007); Kawai et al. (2010)), to damp out these spurious oscillations and enable the use of high-order compact schemes in such flows. Kawai et al. (2010) used the normal stationary shock problem to determine appropriate artificial coefficients for air. A similar systematic assessment for stiffened gases and solids was carried out here, as reported below.

The stiffened gas EOS involves two parameters, p_∞ and γ, with typical values $(p_\infty, \gamma) = (0, 1.4)$ for air, $(6 \times 10^8$ Pa$, 4.4)$ for water and $\gamma = 2 \sim 4$ for metals. Assuming the upstream pressure $p_1 = 10^5$ Pa, the non-dimensional values p_∞/p_1 become 0 and 6×10^3 for air and water, respectively. The Rankine-Hugoniot conditions across a normal stationary shock are

$$\rho_2 u_2 = \rho_1 u_1,$$
$$\rho_2 u_2^2 - \sigma_{11,2} = \rho_1 u_1^2 - \sigma_{11,1},$$
$$\left[\rho_2 \left(\varepsilon_2 + \frac{1}{2}u_2^2\right) - \sigma_{11,2}\right] u_2 = \left[\rho_1 \left(\varepsilon_1 + \frac{1}{2}u_1^2\right) - \sigma_{11,1}\right] u_1,$$

where 1 and 2 denote states upstream and downstream of the shock respectively. For a stiffened gas EOS, these equations can be solved to yield

$$u_2 = \frac{2\gamma\left(p_1 + p_\infty\right) + \left(\gamma - 1\right)\rho_1 u_1^2}{\left(\gamma + 1\right)\rho_1 u_1}, \tag{3.3}$$

$$p_2 = \frac{2\rho_1 u_1^2 - 2\gamma p_\infty - \left(\gamma - 1\right)p_1}{\left(\gamma + 1\right)}, \tag{3.4}$$

$$\rho_2 = \rho_1 u_1 / u_2. \tag{3.5}$$

Non-dimensionalizing the problem using the upstream pressure and density, so that $p_1 = 1$, $\rho_1 = 1$, gave the pressure jump p_2/p_1, as the only parameter defining the problem.

The optimal values of the artificial property coefficients may be expected to depend on the EOS parameters and the non-dimensional problem parameter,

$$(C_\mu, C_\beta, C_k, C_D, C_Y)_{opt} = f(p_\infty/p_1, \gamma, p_2/p_1), \tag{3.6}$$

where the first three coefficients correspond to artificial shear and bulk viscosities and thermal conductivity, respectively, and the last two to the artificial species diffusivity. Following previous attempts (Cook 2007; Kawai et al. 2010) at tuning these coefficients, the values for $C_\mu = 0.002$, $C_\kappa = 0.01$, $C_D = 0.001$, $C_Y = 100$ were fixed and the effect of varying C_β on the solution was examined here.

Figure 2(a) shows profiles of pressure with $(p_\infty/p_1, \gamma, p_2/p_1) = (0, 1.4, 4.5)$, and for varying values of C_β. It is clear that increasing the artificial coefficient value reduces the amplitude of wiggles and increases the shock thickness, making the shock smoother with increasing diffusivity. Similar to Kawai et al. (2010), the wiggles amplitude (A, expressed as a percentage of the pressure jump) was used to quantify the oscillations in this study. Variation of A with the EOS and problem parameter values is depicted in Figure 2(b)-(d). Briefly, Figure 2(b) shows that $C_\beta \sim 1 - 2$ is adequate to keep the amplitudes around 1% for ideal gases, i.e., $p_\infty/p_1 = 0$. The value of C_β required to keep $A \sim 1\%$ increases by about an order of magnitude on increasing p_∞/p_1 to 10^3, keeping γ and p_2/p_1 unchanged. Figure 2(c) shows that A varies from about $1\% - 5\%$ as γ varies from 1.4 to 4.0. Finally, the wiggles amplitude can vary over approximately an order of magnitude as p_2/p_1 varies moderately, depending on the other parameter values.

This study indicated that the appropriate value for C_β in general increases with p_∞/p_1, but is highly dependent on all EOS and problem parameters. The artificial coefficient values necessary for stiffened gas and solid computations deviate significantly from the values used in previous studies for ideal gases. In the elastic-plastic single and multi-material problems discussed below, a C_β value of 17.5, or 10 times larger than the value used for ideal gases, was used.

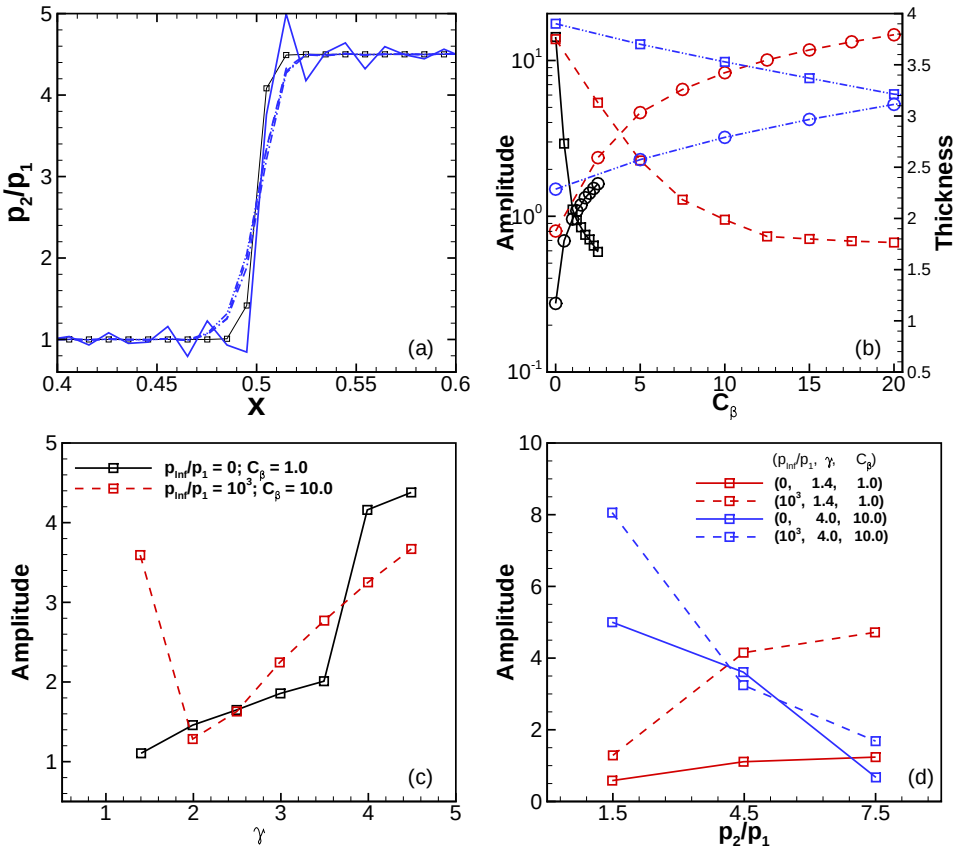

FIGURE 2. (a) Pressure jump for various values of $C_\beta = 0,\ 0.5,\ 1.0$ and 2.0, $p_2/p_1 = 4.5, p_\infty/p_1 = 0, \gamma = 1.4$. (b) Amplitude (lines with squares) and shock thickness (lines with circles) vs C_β for $p_2/p_1 = 4.5, \gamma = 1.4$ and $p_\infty/p_1 = 0$ (solid black lines), 10^3 (dashed red lines) and 6×10^3 (dash-dotted blue lines). (c) Variation in A with fixed $p_2/p_1 = 4.5$, varying γ and (d) with varying p_2/p_1. Other parameters are as indicated on the plots. Numerical parameters were $NX = 101$ and $CFL = 0.5$.

3.3. *Finite waves in elastic solids*

A few one-dimensional test problems demonstrating the full elastic-plastic algorithm described above are discussed briefly in this section. We consider two plates directed towards each other, and impacting at $t = 0$ at the location $x = 0.5$. Such a normal collision of plates leads to compression of the material in the vicinity of the impact, with compression waves traveling away from the interface. In the test problems below, the boundaries were considered to be non-periodic and the simulations were stopped before the waves reached the boundaries. Computation of simple one-sided compact derivatives was sufficient, and no further special treatment was necessary for these 'passive' boundaries.

Results of the single material algorithm are shown in Figures 3(a) and (b). Density and normal velocity snapshots at $t = 0.1$ ms are shown for three different velocities of impact. The material used was steel with properties noted in Table 1. For impact velocity ± 50 m/s, the yield stress was not exceeded, and the solution consisted of only elastic compression waves. For impact velocities ± 150 m/s and ± 300 m/s, the yield stress was

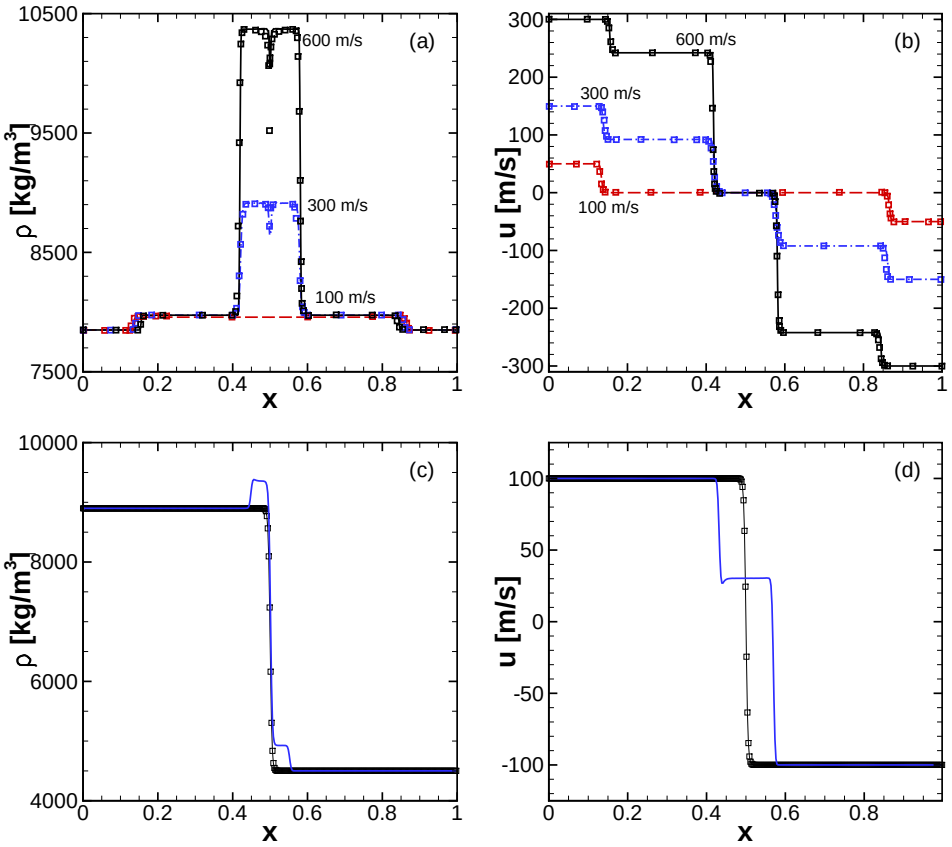

FIGURE 3. (a) Density and (b) velocity profiles at $t = 0.1$ ms in single material elastic-plastic impact problems with different impact velocities. The material was steel with properties in Table 1. (c) Density and (d) velocity profiles at $t = 50\mu$s in a multi-material elastic impact problem. Materials on the left and right of the interface were 'S1' and 'S2' with properties in Table 1. Numerical parameters were $NX = 401$ and $CFL = 0.7$.

.

exceeded, and the solution consisted of an elastic precursor followed by a slower plastic shock wave, on either side of the interface. Figures 3(a) and (b) also show that the results agreed well with those reported in Favrie & Gavrilyuk (2011).

A multi-material impact problem is shown in Figures 3(c) and (d). The materials deoted 'S1' and 'S2' in table 1 were used on the left and right of the interface, respectively. Density and velocity profiles at $t = 0.05$ ms are shown. The solution is similar to the single material impact problems, except for the non-zero velocity at the interface, and the unequal shock strengths and shock propagation speeds in the two materials. Only elastic waves are seen in this problem, since the yield limit is set to infinity.

Similar tests involving elastic-plastic shear waves and elastic-plastic expansion waves were also carried out and found to be in good agreement with reference results. Evaluation of the algorithm in further multi-material problems is currently under way.

4. Conclusions and perspectives

The overall goal of this project is to enable high-order Eulerian simulations of high energy density solid-fluid systems undergoing large deformations in a robust and accurate manner. A fully Eulerian formulation is expected to help overcome difficulties usually encountered in simulations of large deformations using Lagrangian or coupled Lagrangian-Eulerian frameworks. High-order compact schemes are expected to provide accurate simulations with minimal numerical dissipation, unlike previous attempts using dissipative WENO or Godunov-type schemes. High-order accuracy is also expected to help keep computational costs to a manageable level. The formulation and preliminary results outlined above point to several interesting issues that need to be addressed. Three specific issues are discussed briefly.

The separable EOS, with appropriately chosen values for the parameters γ, p_∞ and μ, was designed by, e.g., Kluth & Despres (2008), to provide correct elastic behavior of materials subjected to large strains. Under infinitesimal strains, this EOS should reduce to Hooke's law, which governs linear deformations in materials. For several parameter values typically used in literature to mimic metals such as steel, however, the behavior was found to mimic that of materials with negative Poisson's ratio. While the Poisson's ratio can theoretically vary between 0.5 and -1, metal alloys such as steel have Poisson's ratios of around $0.3 - 0.4$. The EOS in its current form and with the coefficient values typically used in previous studies is not always meaningful in the linear, elastic limit. Alternative forms for the elastic component of internal energy and various parameter values need to be explored for their ability to succesfully yield qualitatively and quantitatively correct behavior under both infinitesimal and finite strains.

The use of compact schemes based on central-differences leads to spurious oscillations in the presence of shocks. Artificial fluid properties are necessary to damp out these oscillations and provide stable and accurate simulations. Previously, artificial fluid properties have mainly been used for simulations of ideal gases, most commonly air. The coefficients used for artificial properties did not need to be tuned depending on the various test problems involving air. Our preliminary simulations revealed that the coefficient values commonly used for air need to be modified significantly depending on the EOS parameters as well as problem parameters. The use of centered compact-difference schemes can also lead to the species volume fractions, species masses and species hydrodynamic energies going negative occasionally. Although these issues were not encountered in the simple problems outlined in this paper, tuning of artificial coefficients and incorporation of additional artificial source terms might be needed in order to ensure positivity in problems involving large property jumps. Nevertheless, it is encouraging that a numerical framework comprised of high-order compact schemes with artificial fluid properties works well for liquids and solids as well as gases, and this presents an opportunity for a unified treatment of discontinuities in various continuum media.

The current formulation for plasticity is based on the J_2-flow theory for isotropic materials, with the assumptions that the plastic deformations are volume preserving, and act to relax the tangential stresses (Barton et al. 2013). This reduces the number of variables that need to be evolved, but restricts the spectrum of plastic deformations that can be modeled. As pointed out in Miller & Colella (2001), capturing truly plastic behavior requires advancing the full inverse deformation gradient tensor, g_{ij} as well as its plastic part, g^p_{ij}. The effect of these simplifying assumptions needs to be assessed carefully via comparisons to appropriate experiments, and extension or modification of

the current formulation to account for more complex plastic deformations needs to be explored.

Resolution of the issues identified by the preliminary tests outlined here, implementation in two and three dimensions, comparisons to experimental and other numerical results, followed by application to practical problems are planned in the future.

Acknowledgments

This investigation was funded by Grant # B612155 from the Lawrence Livermore National Laboratory, US Department of Energy. The authors would like to thank Dr. Evan Gawlik for several insightful comments that led to substantial improvements to this report.

REFERENCES

Barton, P. T., Deiterding, R., Meiron, D. I. & Pullin, D. I. 2013 Eulerian adaptive finite-difference method for high-velocity impact and penetration problems. *J. Comput. Phys.* **240**, 76–99.

Barton, P. T., Drikakis, D., Romenski, E. & Titarev, V. A. 2009 Exact and approximate solutions of Riemann problems in non-linear elasticity. *J. Comput. Phys.* **228**, 7046–7068.

Bhagatwala, A. & Lele, S. K. 2009 A modified artificial viscosity approach for compressible turbulence simulations. *J. Comput. Phys.* **228**, 4965–4969.

Cook, A. W. 2007 Artificial fluid properties for large-eddy simulation of compressible turbulent mixing. *Phys. Fluids* **19**, 055103.

Cook, A. W. & Cabot, W. H. 2004 A high-wavenumber viscosity for high-resolution numerical methods. *J. Comput. Phys.* **195**, 594–601.

Dorovskii, V. N., Iskoldskii, A. M. & Romenskii, E. I. 1983 Dynamics of impulsive metal heating by a current and electical explosion of conductors. *J. Appl. Mech. Tech. Phy.* **24**, 454–467.

Favrie, N. & Gavrilyuk, S. L. 2010 Dynamics of shock waves in elastic-plastic solids. *ESAIM Proceedings* pp. 1–18.

Favrie, N. & Gavrilyuk, S. L. 2011 Mathematical and numerical model for nonlinear viscoplasticity. *Phil. Trans. Royal Soc. A* **369**, 2864–2880.

Favrie, N. & Gavrilyuk, S. L. 2012 Diffuse interface model for compressible fluid - compressible elastic-plastic solid interaction. *J. Comput. Phys.* **231**, 2695–2723.

Gavrilyuk, S. L., Favrie, N. & Saurel, R. 2008 Modelling wave dynamics of compressible elastic materials. *J. Comput. Phys.* **227**, 2941–2969.

Hill, D. J., Pullin, D. I., Ortiz, M. & Meiron, D. I. 2010 An Eulerian hybrid WENO centered-difference solver for elastic-plastic solids. *J. Comput. Phys.* **229**, 9053–9072.

Kawai, S., Shankar, S. K. & Lele, S. K. 2010 Assessment of localized artficial diffusivity scheme for large-eddy simulation of compressible turbulent flows. *J. Comput. Phys.* **229**, 1739–1762.

Kluth, G. & Despres, B. 2008 Perfect plasticity and hyperelastic models for isotropic materials. *Contin. Mech. and Thermodyn.* **20**, 173–192.

Lele, S. K. 1992 Compact Finite Difference Schemes with Spectral-like Resolution. *J. Comput. Phys.* **103**, 16–42.

López Ortega, A., Lombardini, M., Pullin, D. I. & Meiron, D. I. 2014 Numerical simulation of elastic-plastic solid mechanics using an Eulerian stretch tensor approach and HLLD Riemann solver. *J. Comput. Phys.* **257**, 414–441.

Mani, A., Larsson, J. & Moin, P. 2009 Suitability of artificial bulk viscosity for large-eddy simulation of turbulent flows with shocks. *J. Comput. Phys.* **228**, 7368–7374.

Miller, G. H. & Colella, P. 2001 A High-Order Eulerian Godunov Method for Elastic-Plastic Flow in Solids. *J. Comput. Phys.* **167**, 131–176.

Ndanou, S., Favrie, N. & Gavrilyuk, S. L. 2015 Multi-solid multi-fluid diffuse interface model: Applications to dynamic fracture and fragmentation. *J. Comput. Phys.* **295**, 523–555.

Olson, B. J. & Lele, S. K. 2011 Directional artificial fluid properties for compressible large-eddy simulation. *J. Comput. Phys.* **246**, 207–220.

Plohr, B. & Sharp, D. 1989 A Conservative Eulerian Formulation of the Equations for Elastic Flow. *Adv. in Appl. Math.* **9**, 481–499.

Plohr, B. & Sharp, D. 1992 A Conservative Formulation for Plasticity. *Adv. in Appl. Math.* **13**, 462–493.

Saurel, R., Petitpas, F. & Berry, R. 2009 Simple and efficient relaxation methods for interfaces separating compressible fluids, cavitating flows and shocks in multiphase mixtures. *J. Comput. Phys.* **228**, 1678–1712.

Trangenstein, J. A. & Colella, P. 1991 A Higher-Order Godunov Method for Modelling Finite Deformation in Elastic-Plastic Solids. *Comm. Pure Appl. Math.* **44**, 41–100.

Tritschler, V. K., Olson, B. J., Lele, S. K., Hickel, S., Hu, X. Y. & Adams, N. A. 2014 On the Richtmyer-Meshkov instability evolving from a deterministic multimode planar interface. *J. Fluid Mech.* **755**, 429–462.